Pharmaceutical Research, Vol. 24, No. 3, March 2007 (© 2007)
DOI: 10.1007/s11095-006-9169-0

Research Paper

Solubility-Excipient Classification Gradient Maps

Alex Avdeef,[1,3] Stefanie Bendels,[2] Oksana Tsinman,[1] Konstantin Tsinman,[1] and Manfred Kansy[2]

Received July 27, 2006; accepted September 19, 2006; published online January 24, 2007

Abstract. This study assessed the effect of excipients (sodium taurocholate, 2-hydroxypropyl-β-cyclodextrin, potassium chloride, propylene glycol, 1-methyl-2-pyrrolidone, and polyethylene glycol 400) on the apparent intrinsic solubility properties of eight sparingly soluble drugs (four bases, two neutrals, and two acids): astemizole, butacaine, clotrimazole, dipyridamole, griseofulvin, progesterone, glibenclamide, and mefenemic acid. Over 1,200 UV-based solubility measurements (pH 3–10) were made with a high-throughput instrument. New equations, based on the "shift-in-pK_a" method, were derived to interpret the complicated solubility–pH dependence observed, and poorly predicted by the Henderson–Hasselbalch equation. An intrinsic solubility-excipient classification gradient map visualization tool was developed to rank order the compounds and the excipients. In excipient-free solutions, all of the ionizable compounds formed either uncharged or mixed-charge aggregates. Mefenamic acid formed anionic dimers and trimers. Glibenclamide displayed a tendency to form monoanionic dimers. Dipyridamole and butacaine tended to form uncharged aggregates. With strong excipients, the tendency to form aggregates diminished, except in the case of glibenclamide. We conclude that a low-cost, compound-sparing, and reasonably accurate high-throughput assay which can be used in early screening to prioritize candidate molecules by their eventual developability via the excipient route is possible with the aid of the "self-organized" intrinsic solubility-excipient classification gradient maps.

KEY WORDS: Double-Sink PAMPA; excipients; HP-β-CD; intrinsic solubility-excipient mapping; low solubility; methylpyrrolidone; propylene glycol; PEG400; sodium taurocholate.

INTRODUCTION

The rate and extent of entry of an orally delivered drug from the gastrointestinal luminal fluid into the blood stream depends on many physicochemical factors that impact on solubility, permeability, and charge state of the drug (1–3). Large, polar/ionized molecules are usually poorly absorbed because of low permeability across the gastrointestinal tract (GIT) barrier. But molecules with high intrinsic permeability can also be poorly absorbed, if their aqueous solubility is extremely low.

Combinatorial chemistry programs often tend to select for high molecular weight molecules, which are predictably low in solubility. 'Early warning' tools, such as Lipinski's 'Rule of 5' (4,5), and computer programs that predict solubility from 2-D structures (6–8), attempt to weed out such molecules early in discovery programs. Although the popular turbidity-based kinetic solubility measurements (4,5) are fast, it is arguable whether their accuracy is any better than that of computational prediction methods (9,10). Many solubility-problematic molecules remain unrecognized for a long time as such, due to the overly simplistic methods used to measure solubility, and the masking effect of organic solvents (e.g., DMSO) used in discovery measurements (9). When candidate molecules with extremely low solubility are selected for development, often it is not practical to chemically alter these otherwise active molecules. Formulation efforts with such compounds may be expensive, time consuming, and not always successful (10). During candidate selection, usually, low-solubility molecules are not screened for their future formulation efficacy.

Glomme *et al.* (9) and Bergström *et al.* (11) made persuasive arguments for early application of accurate, compound-sparing, and fast methods to determine solubility, based on miniaturized shake-flask measurements. In particular, effects of pH and excipients (particularly biorelevant bile salts) on solubility could further optimize the final candidate selection (9,12). In the case of sparingly soluble, but otherwise promising molecules, first-round excipient screening, perhaps preceding preclinical development, could be used to prioritize the selected molecules and perhaps minimize the number of early animal studies.

However, accurate measurement of solubility of sparingly soluble drugs is challenging, for a number of reasons (13–26). For example, the intrinsic solubility of amiodarone

Contribution number 22 in the *PAMPA—a Drug Absorption in vitro Model* series from *p*ION. (29) is part 21 in the series. Double-Sink PAMPA™, PAMPA-Mapping™, and ISE-Mapping™ are trademarks of pION INC.

[1] *p*ION INC, 5 Constitution Way Woburn, MA 01801, USA.
[2] Pharmaceutical Division, F. Hoffmann-La Roche Ltd., PRBD-E, CH-4070 Basel, Switzerland.
[3] To whom correspondence should be addresed. (e-mail: aavdeef@pion-inc.com)

(3,9,11) is onerous to measure accurately, in part because of the tendency of the drug to form multiple metastable gels, which can persist for as long as a month (18). Aggregation (14–16) and micelle formation (17,18), common with low-solubility molecules, can hamper the interpretation of the measurements. Roseman and Yalkowsky (19) described the solubility–pH behavior of prostaglandin F2α and noted that anionic aggregates appeared to form (Case 2a in "THEORETICAL SECTION"), since the ascending portion of the solubility–pH curve was shifted to lower pH values than predicted by the Henderson–Hasselbalch equation. Many nonsteroidal antiinflammatory drugs (17), such as indomethacin (21), diclofenac, ibuprofen, ketoprofen, naproxen, and sulindac, can self-associate by forming mixed-charge micelle or micelle-like structures (Cases 1a and 3 below). Zhu and Streng (15) found that the self-association of dolasetron to form cationic dimers and trimers (Case 2b below) was enthalpy-driven (H-bond and/or π–π interactions), not by hydrophobic/electrostatic interactions, with the aggregation constants, log K_{2-3}, ranging from 0.6 to 1.7 (M^{-1} scale, cf., "THEORETICAL SECTION"). Decamers with log K_{10}=12.1 were observed for MDL201346A by Streng *et al.* (14). Such aggregates were found to have unusually high solubility and/or solubility very sensitive to temperature. Jinno *et al.* (20) showed how the excipient sodium lauryl sulfate (SLS) affects the solubility–pH profile of piroxicam. Avdeef *et al.* (21) proposed a computational model, based on the of "shift in the apparent pK_a" method (3,21–24), to rationalize the SLS effect on the solubility of piroxicam (Case 1a below). The dimeric association constant of piroxicam at 37°C, $1.7\times10^{+3}$ M^{-1}, increased to $35\times10^{+3}$ M^{-1} at 25°C (21). Solubilizing complexing agents, such as cyclodextrins, can have multiple stoichiometries of association, making interpretations of the phase-solubility diagrams burdensome (25,26). Bergström *et al.* (11) accurately characterized the solubility–pH profiles of 25 sparingly soluble amine drugs, and observed that the Henderson–Hasselbalch equation was very unreliable in predicting the pH-dependence of solubility of these compounds. Aggregation equilibria surely played a role, although this was not investigated in detail.

The reliable and accurate measurement of solubility in the above examples requires much effort. Since so many molecules in discovery programs have very low solubility, measurement of solubility needs to be both rapid and compound-sparing. Screening for excipient effects makes the task further daunting, and this is seldom done in discovery. Nevertheless, rapid methods of systematic screening for solubilizing agents are emerging (27–29). Chen *et al.* (28) used full factorial robotic assay to screen about 10,000 combinations of 12 excipients (including PEG400, polysorbate 80, and ethanol) in a number of combinations to discover an improved Cremophor EL-free formulation for paclitaxel, a well established marketed drug. There clearly are opportunities to improve both the efficiency and the accuracy of such rapid methods, using partial factorial design-of-experiments (DOE). Commercial software linking DOE approaches directly to robotic control exist (30–32). Also, there are opportunities to automate computational methods to properly treat the solubility data for possible aggregation effects.

In this study, we propose to extend to solubility-excipient measurement, the theme explored in a previous Double-Sink PAMPA excipient study (29), where we introduced the method of PAMPA-Mapping, based on eight sparingly soluble drugs (astemizole, butacaine, clotrimazole, dipyridamole, griseofulvin, progesterone, glibenclamide, and mefenemic acid), measured under 15 combinations of six excipients (sodium taurocholate, 2-hydroxypropyl-β-cyclodextrin, potassium chloride, propylene glycol, 1-methyl-2-pyrrolidone (33), and polyethylene glycol 400 (34)). Our aim was to develop a practical and cost-effective high-throughput (microtitre plate) assay, both compound-sparing and minimally compromising on accuracy, which could be used in early screening for solubility under GIT-relevant conditions of excipients.

MATERIALS AND METHODS

Drugs and Chemicals

The eight model compounds used in this study were purchased from Sigma–Aldrich (St. Louis, MO, USA). The pH of the assayed donor solutions was adjusted with universal buffers (*p*ION, PN 100621, 1100151), whose ionic strength is 0.01 M. Excipients were purchased from Sigma–Aldrich (St. Louis, MO, USA) except polyethylene glycol 400 (PEG 400), which was purchased from EM Science (VWR).

Excipient Concentrations

Quantities of the six excipients were selected to overlap the concentrations expected in the gastrointestinal fluid under clinically relevant conditions, as described previously (29). Briefly, KCl was selected at 0.1 and 0.2 M; sodium taurocholate (NaTC) solutions were prepared at 3 and 15 mM, corresponding to fasted and fed GIT states (35). For liquid excipients, the maximum capsule volume was assumed to be 0.6 ml: for a GIT volume of 250 ml (35), the calculated excipient concentration is 0.24% v/v. Hence, for *N*-methylpyrrilidone (NMP), propylene glycol (PG), and polyethylene glycol 400 (PEG400), excipient solutions of 0.24, 1, and 5% v/v were tested. With encapsulated solid excipients, such as hydroxypropyl-β-cyclodextrin (HP-β-CD), with MW 1,396 and solubility 450 mg/ml, it should be possible to pack 270 mg into a 0.6 ml capsule, which is equivalent to a 0.1% w/v solution in the GIT volume. Slightly higher values of 0.24 and 1% w/v were used in the study. In all, counting the excipient-free buffer solutions, 15 different solutions were tested with the eight drug molecules for the effect on solubility, resulting in 120 drug-excipient combinations, with about 1,200 individual solubility–pH measurements.

pK_a Measurement

The high-precision pK_a data, determined by the potentiometric method using the Gemini instrument (*p*ION), were taken from Bendels *et al.* (29). These were determined by extrapolation in methanol–water solutions, taking advantage of the Gemini's capability to determine pK_a values even if there is precipitation during a portion of the titration, in either aqueous or cosolvent solutions. The pH electrode calibration was performed "*in situ*" by the instrument, concurrently with the pK_a determination, especially an important novel feature for pK_a<3 or >10 in cosolvent solutions (29).

Micro Solubility Method

The highly automated direct-UV 96-well microtitre plate equilibrium solubility method (22) in the μSOL Evolution instrument from *p*ION INC (Woburn, MA, USA) was used in this study, with data collected at room temperature (25±2°C). Samples are typically introduced as 10–30 mM DMSO solutions. The robotic liquid handling system (e.g., Beckman Coulter Biomek-FX® ADMETox Workstation or Tecan Freedom Evo® Workstation) draws a 3–10 μl aliquot of the DMSO stock solution and mixes it into an aqueous universal buffer solution, so that the final (maximum) sample concentration is 50–250 μM in the excipient-containing buffer solutions. The residual DMSO concentration was kept at 1.0% (v/v) in the final buffer solutions. The solutions were varied in pH (NaOH-treated universal buffer). This pH variation is necessary in order to determine the aggregation and intrinsic solubility constants (21). The order of solution additions was: (a) for excipient-free solutions, the universal buffer (initially at pH 3) was adjusted in pH with NaOH; (b) for solutions containing excipients, the buffer was freshly prepared with the desired level of excipient added; (c) aliquots of the DMSO stock solution were then added to the buffer solutions in a deep-well plate; (d) the solutions were thoroughly mixed on the robotic workstation. Each solubility–pH measurement was performed in duplicate, and the results were averaged by the instrument software. The buffers used in the assay are automatically prepared by the robotic system. The quality controls of the buffers and the pH electrode are performed by alkalimetric titration, incorporating the Avdeef–Bucher (36) procedure. After 18±1 h, the buffer solutions containing suspensions of the drug solid were filtered (0.2 μm pore microfilter), and the supernatant solutions were assayed for the amount of material present, by comparison with UV spectra (230 to 500 nm) obtained from a reference standards, using a proprietary spectroscopic procedure that comes with the Evolution instrument. The automated procedure can determine if no solid had formed in the assayed solutions, by comparing the expected concentration to the observed concentration. The precipitate which formed was not analyzed for its crystalline characteristics in the high-throughput procedure, although this can be done when necessary.

The filtration technique used prior to the UV quantitation step was the "dual-step" type, where an aliquot of the solution containing solid was slowly filtered, with the aim to allow the filter material to saturate with the tested compound. This first filtrate was discarded. The second filtration step was analytically improved, since the surface of the hydrophilic filter material was pre-saturated with the compound.

THEORETICAL SECTION

Case 1a, 1b, 2a and 2b Aggregates: $(HA)_n$, B_n, $(A^-)_n$, $(BH^+)_n$

When a compound forms a dimer or a higher order oligomer in aqueous solution, the characteristic solubility–pH profile takes on a shape not predicted by the Henderson–Hasselbalch equation (cf., solid curves in Fig. 1), and often indicates an *apparent* pK_a that is different from the true pK_a (e.g., Cases 1a and 1b in Fig. 1), as determined potentiometrically in dilute aqueous or cosolvent solutions (29). Figure 1 shows six different cases of aggregation-induced distortions of log *S*–pH curves, where *S* stands for solubility (molarity or μg/ml units here). Derivations of Cases 1a, 1b, 2a and 2b have been described in the literature, and preliminary methods to extract underlying intrinsic solubility values have been discussed (3,21,23,24). Cases 3a and 3ax treatments are new, and their derivations are briefly described below. Based on such pK_a-shift in solubility analysis, dimerization constants ranging from $1.7\times10^{+3}$ to $1.8\times10^{+5}$ M^{-1} were proposed (21) for phenazopyridine (Case 2b), indomethacin (Case 2a), 2-naphthoic acid (Case 2a), and piroxicam (Case 1a).

The equations summarized in this study mathematically describe solubility–pH relationships, and can be used for the practical purpose of data interpolation, extrapolation, smoothing, and compaction (whole curves described with minimal number of constants). Furthermore, the pK_a-shift method can be used as a quick alert tool. (As is implied, the molecule must have an ionization group within the accessible pH range, in order for the method to work.) When a log *S vs.* pH plot is inspected, and the true pK_a is known independently, it can be quickly surmised whether aggregates are present, and whether these "anomaly" effects are due to the neutral or the charged form of the drug. Moreover, the intrinsic solubility may be calculated from the magnitude or the direction of the pK_a shift. Caution is needed not to mechanistically over-interpret the measurement data, however (21). If an uncharged molecule undergoes some speciation anomaly (aggregation, DMSO binding, filter retention, etc.), weak acids will indicate an apparent pK_a higher than the true pK_a (Case 1a), and weak bases will indicate an apparent pK_a lower than the true pK_a (Case 1b). If the observed shifts are opposite of what's stated above, then the charged (rather than the neutral) species is involved in the anomaly (Cases 2a and 2b). Although the precise mechanism of the anomaly may not be apparent in all cases, the shift combined with the apparent solubility will often reveal the intrinsic solubility, S_o. There is a further practical consequence to this with excipients: it is possible in many instances to measure solubility in the presence of excipients and at the same time to assess the solubility that would have been evident in the absence of added excipients, as though they were the source of anomaly (e.g., piroxicam in (21)).

Table I summarizes the solubility–pH equations derived below and those previously published (21). Six types of aggregates: $(HA)_n$, B_n, A_n^{n-}, $(BH^+)_n$, $(AH\cdot A)_n^{n-}$, and $(AH\cdot A)_n^{n-}$ in the presence of excipients are considered. Their derivations follow along the lines reported in the literature (3,21–24). This is briefly summarized below for the two new cases.

Mixed-Charge Weak Acid Aggregates, $(AH\cdot A)_n^{n-}$ (Case 3a)

In Cases 2a and 2b, the order of aggregation is revealed by slopes greater than one in the log *S*–pH plots (21). In the present study, we discovered several instances of slopes being near one, even though some sort of aggregation was apparently taking place. We now have a plausible model to describe this case. We can hypothesize that the oligomeric mixed-charge weak acid species, $(AH\cdot A)_n^{n-}$, forms, which

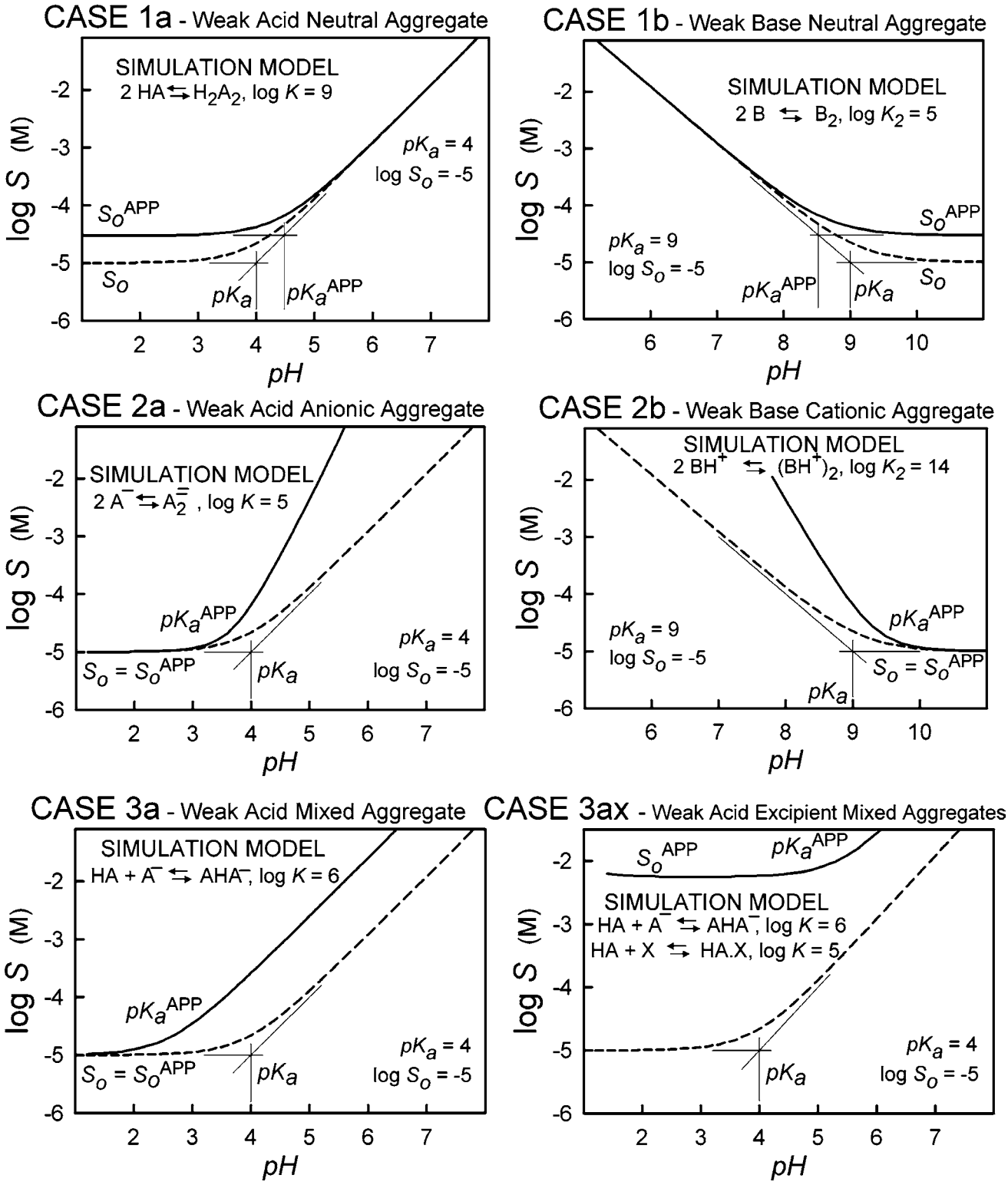

Fig. 1. Plots of log solubility *vs.* pH involving six cases of aggregation equilibrium. See Table I for the equations represented by the *solid curves*. The *dashed curves* were calculated with the Henderson–Hasselbalch equation, using the true pK_a values. The simulation calculations were based on assumed pK_a=4 for acids and pK_a=9 for bases, with log S_0=5 (S_0 is intrinsic solubility, molarity scale) in all cases. The aggregation constants selected for each case are indicated by log K values.

Table I. Solubility Equations for Aggregates

Case	Aggregate Equilibrium	log S	
		General Form	Two Limiting Linear Segments
1a	$n\,HA \rightleftarrows (HA)_n$	$= \log S_o + \log\left(1 + K_a/[H^+] + n\,K_n^{o} S_o^{n-1}\right)$	$= \log S_o + \log\left(1 + n\,K_n^{o} S_o^{n-1}\right)$ $= \log S_o^{APP}$@pH $\ll pK_a$ $= \log S_o - pK_a + pH$@pH $\gg pK_a^{APP}$
1b	$n\,B \rightleftarrows (B)n$	$= \log S_o + \log\left(1 + [H^+]/K_a + n\,K_n^{o} S_o^{n-1}\right)$	$= \log S_o + \log\left(1 + n\,K_n^{o} S_o^{n-1}\right)$ $= \log S_o^{APP}$@pH $\gg pK_a$ $= \log S_o + pK_a - pH$@pH $\ll pK_a^{APP}$
2a	$n\,A^- \rightleftarrows (A^-)_n$	$= \log S_o + \log\left(1 + K_a/[H^+] + n\,K_n^{\ominus} K_a^n S_o^{n-1}/[H^+]^n\right)$	$= \log S_o = \log S_o^{APP}$@pH $\ll pK_a^{APP}$ $= \log n + \log K_n^{\ominus} + n(\log S_o - pK_a)$ $+ n$ pH@pH $\gg pK_a$
2b	$n\,BH^+ \rightleftarrows (BH^+)_n$	$= \log S_o + \log\left(1 + [H^+]/K_a + n\,K_n^{\oplus}[H^+]^n S_o^{n-1} / K_a^n\right)$	$= \log S_o = \log S_o^{APP}$@pH $\gg pK_a^{APP}$ $= \log n + \log K_n^{\oplus} + n(\log S_o + pK_a)$ $- n$ pH@pH $\ll pK_a$
3a	$n\,A^- + n\,HA \rightleftarrows (AH \cdot A^-)_n$	$= \log S_o + \log\left(1 + K_a/[H^+] + 2n\,K_n^{*} K_a^n S_o^{2n-1} / [H^+]^n\right)$	$= \log S_o = \log S_{o*}^{APP}$@pH $\ll pK_o^{APP}$ $= \log 2n + \log K_n^{*} + 2n \log S_o - n\,pK_a$ $+ n$ pH@pH $\gg pK_a$
3ax	$n\,A^- + n\,HA \rightleftarrows (AH \cdot A^-)_n$ &$HA + X \rightleftarrows HA \cdot X$	$= \log S_o + \log\left(1 + K_a/[H^+] + 2n\,K_n^{*} K_a^n S_o^{2n-1} / [H^+]^n + K^{\boxtimes}\right)$	

contains a 1:1 ratio of HA and A^-. The required equilibrium equations and the associated concentration quotients to completely define the mass balance problem are

$$HA \leftrightarrows H^+ + A^- \qquad K_a = [H^+][A^-] / [HA] \tag{1a}$$

$$HA(s) \leftrightarrows HA \qquad S_0 = [HA] \tag{1b}$$

$$n A^- + n\,HA \leftrightarrows (AH \cdot A)_n^{n-}$$
$$K_n^{*} = \left[(AH \cdot A)_n^{n-}\right] \Big/ [HA]^n [A^-]^n \tag{2}$$

Solubility is defined by

$$S = [A^-] + [HA] + 2n\left[(AH \cdot A)_n^{n-}\right] \tag{3}$$

The $[A^-]$ and $[(AH{\cdot}A)_n^{n-}]$ components in Eq. 3 may be expanded in terms of [HA], pH, and the various equilibrium constants:

$$\begin{aligned} S &= [HA]\,K_a/[H^+] + [HA] + 2n\,K_n^{*}[A^-]^n[HA]^n \\ &= [HA]\left\{K_a/[H^+] + 1 + 2n\,K_n^{*} K_a^n [HA]^{2n-1} \Big/ [H^+]^n\right\} \end{aligned} \tag{4}$$

In logarithmic general form (cf., Table I),

$$\log S = \log S_o + \log\left(1 + K_a/[H^+] + 2n\,K_n^{*} K_a^n S_o^{2n-1}/[H^+]^n\right) \tag{5}$$

Two limiting forms of Eq. 5 may be posed as

$$\log S = \log S_o \qquad @pH \ll pK_a^{APP} \tag{6a}$$

$$\log S = \log 2n + \log K_n^{*} + 2n \cdot \log S_o - n\,pK_a + n\,pH \qquad @pH \gg pK_a \tag{6b}$$

Equation 6a indicates that the formation of mixed-charge aggregates does not obscure the value of the intrinsic solubility in low pH solutions (cf., Case 3a in Fig. 1). If for a weak acid, whose *apparent* pK_a in a saturated solution is less than the true pK_a, a slope of +1 for pH>>pK_a in a log S *vs.* pH plot is consistent with the formation of the *dimeric* species $AH{\cdot}A^-$. A slope of +2, however, could indicate a Case 2a dimer or a Case 3a tetramer, which may be difficult to discern.

Mixed-Charge Aggregates, $(AH \cdot A)_n^{n-}$, *in the Presence of Excipient X (CASE 3ax)*

In Case 3a, the slope in the log S–pH plot cannot be less than one. The cases we observed where the slope was less than one needed further modification to our computation models. We can hypothesize that the oligomeric mixed-charge weak acid species, $(AH \cdot A)_n^{n-}$, forms, in the presence of an excipient, X, which binds only the neutral form of the weak acid HA. In addition to Eqs. 1a, 1b and 2, we need

$$HA + X \leftrightarrows AH \cdot X \qquad K^{\boxtimes} = [AH \cdot X]/[HA] \tag{7}$$

The $K^{\boxtimes}$ equilibrium constant embeds the product of the equilibrium constant for equilibrium expression in Eq. 7 and the concentration of the excipient, X, which is assumed to be practically constant (i.e., $[HA]_{total} << [X]_{total}$). Solubility is defined by

$$S = [A^-] + [HA] + 2n\left[(AH \cdot A)_n^{n-}\right] + [AH \cdot X] \tag{8}$$

As before, the non-[HA] components in Eq. 8 may be expanded in terms of [HA] and the various equilibrium constants, leading to the general form equation (cf., Eq. 5):

$$\log S = \log S_o + \log\left(1 + K_a/[H^+] + 2n\,K_n^{*} K_a^n S_o^{2n-1} / [H^+]^n + K^{\boxtimes}\right) \tag{9}$$

The Case 3ax example in Fig. 1 is based on equilibrium constants indicated in the figure. In general it is not possible to extract limiting forms of the equation, other than to suggest that the slope at extreme pH still needs to be ≥1, because of the *n*-dependence of pH in Eq. 9. As the Case 3ax example in Fig. 1 illustrates, if the measured data are only taken from the bend in the curve at high pH, the slope may *appear* less than one, but if higher-pH data were available, the model would predict a slope of +1.

Refinement of Aggregation Parameters

The solubility–pH data measured by the μSOL Evolution instrument were processed by the onboard software and stored in the ELM™ Data Manager (*p*ION). The data from several different assays, pooled in ELM, were further tested by the software for the presence of aggregates. One of the equations in Table I was automatically selected by the Evolution software.

The strategy used by the software is first to fit the data to the expected Henderson–Hasselbalch equation, from which the apparent pK_a is determined. Depending on the sign of the difference between the true (supplied) and apparent (fitted) ionization constants, the software-equivalent of Fig. 1 is consulted to select the most appropriate case. With the most probable case identified, the appropriate equation in Table I is then applied to a second regression analysis of the data, where the finalized parameters are determined by refinement.

The log *S*–pH data were fitted to it by a weighted nonlinear regression procedure, where the following residual function was minimized,

$$r = \sum_{i}^{N} \frac{\left(\log S_i^{obs} - \log S_i^{calc}\right)^2}{\sigma_i^2(\log S)} \tag{10}$$

where N is the measured number of solubility values in the model, and log S_i^{calc} is the calculated log solubility (Table I equation), which is a function of the refined parameters: pK_a^{APP} (apparent ionization constant), log S_o^{APP} (apparent intrinsic solubility), log S_o (true intrinsic solubility—Cases 1a and 1b only), log K_n (aggregation constant), and n (aggregation order). The estimated standard deviation in the observed log S, σ_i, was estimated as 0.05 (log units). The overall quality of the refinement was assessed by the "goodness-of-fit,"

$$\mathrm{GOF} = \sqrt{\frac{r}{N - N_p}} \tag{11}$$

where N_p is the number of refined parameters.

RESULTS AND DISCUSSION

Table II lists all of the refined results in this study. Underlying the refined values are about 1,200 individual solubility–pH measurements, acquired rapidly by the robotic instrument.

Micro Solubility Measurements without Excipients

Figure 2 shows the log *S*–pH solubility plots under the excipient-free conditions. The dashed curves correspond to those predicted by the Henderson–Hasselbalch equation (using the true pK_a), and are presented as a comparison to the curves more accurately reflecting the solubility–pH dependence. The dotted horizontal line indicates the apparent intrinsic solubility. The solid curve corresponds to the best-fit of the actual data (filled circles), according to one of the equations in Table I. The bases studied here tended to form cationic aggregates (Case 2b), with the exception of butacaine and dipyridamole, which apparently formed neutral aggregates (Case 1b). The two acids studied mostly form anionic aggregates (Case 2a or 3a). It was not possible to apply the "pK_a-shift" method to the non-ionizable compounds, so the degree to which aggregates may form is not known form this study.

Glibenclamide in Fig. 2e is an example of Case 3a in the non-excipient results, since aggregates are suggested by the negative shift of 1.6 log units in the apparent pK_a, and the unit slope in the high-pH data. That is, the data are consistent with the formation of negatively charged dimers, $AH{\cdot}A^-$. Clotrimazole (Fig. 2c) appears to be composed of a combination of $B.BH^+$ and $(BH^+)_2$ species, as suggested by the slope value of n=1.4. Astemizole (Fig. 2a) appears to be composed of dimeric (n=1.8) $(BH^+)_2$ species, whereas mefenamic acid (Fig. 2f) has both dimers and trimers of this type (n=2.6). Dipyridamole and butacaine represent Case 1b behavior, where uncharged aggregates are hypothesized to form, which elevate the apparent solubility above the value expected if no aggregates formed, as that which would be expected from the Henderson–Hasselbalch equation (dash curves). These two molecules are also the most soluble of the ionizable molecules considered. As pointed out elsewhere (21), it is not possible to assess the degree of aggregation (n) from the log *S*–pH data, when Case 1a or 1b dependence is indicated.

It is clear that all of the compounds studied here are sparingly soluble in excipient-free buffer ("none" row in Table II), with mefenamic acid being the least soluble, at 21±5 ng/ml. It may be quite surprising that such a low value can be obtained by a UV-based high-throughput microtitre method. It might be even suggested that the 18 h incubation time used is anything but "high-throughput." But, it must be noted that during a 24 h duty cycle of the instrument, four to ten 96-well plates can be processed. It is this parallel nature of the robotic measurement that makes the overall procedure very fast. The 18 h incubation time increases the probability that the measured results represent the true equilibrium solubility values of the most stable polymorph of the drug, and not the kinetic values of other fast methods, those based on the use of turbidity detection (we will compare our results to more rigorous shake-flask methods later in the discussion).

The intrinsic solubility of astemizole, clotrimazole, and glibenclamide were measured as 0.3–0.4 μg/ml (Table II). The corrected intrinsic solubility of dipyridamole is 2.3±0.7 μg/ml (6.2±1.1 μg/ml apparent value). The nonionizable compounds, griseofulvin and progesterone, are moderately soluble in comparison to the other compounds, measuring 14–17 μg/ml. Butacaine has a corrected intrinsic solubility of 1.9±0.7 μg/ml (40±6 μg/ml apparent value). It is clear from these and other measurements (below) that the sensitivity of the μSOL Evolution method reaches the low nanogram region, in part made possible by the highly developed spectroscopic data processing software in the Evolution instrument.

Table II. Refined Solubility and Aggregation Parameters

Compound	pK_a	Excipient	S_o^{APP}±SD	S_o±SD	log K_n±SD	Case	n±SD	pK_a^{APP}±SD	GOF
Astemizole	8.60	none	0.29±0.08		5.07±0.44	2b	1.8	8.9±0.3	3.0
	5.84	0.1 M KCl	0.19±0.03		5.00±0.21	2b	2.4	9.2±0.6	1.2
		0.2 M KCl	0.27±0.04		4.39±0.27	2b	2.4	8.8±0.4	1.4
		0.24% PG	0.22±0.05		3.17±0.53	2b	3.5	8.7±0.2	2.3
		1% PG	0.22±0.04		3.27±0.41	2b	3.6	8.7±0.4	1.8
		5% PG	0.31±0.07		4.66±0.33	2b	2.2	9.0±0.5	1.8
		0.24% NMP	0.38±0.06		4.89±0.24	2b	2.2	9.1±0.5	1.4
		1% NMP	0.38±0.08		5.67±0.23	2b	1.6	9.3±0.4	1.4
		0.24% PEG400	0.48±0.01		7.50±0.01	2b	1.2	10.6±0.2	0.1
		1% PEG400	0.29		7.11±0.07	2b	1.5	10.0±0.2	1.1
		5% PEG400	0.29		7.87±0.02	2b	1.1	10.8	0.4
		3 mM NaTC	0.63±0.07	0.2±0.1		1b		8.1±0.1	0.9
		15 mM NaTC	3.0±0.7	1.4±0.7		1b		8.3±0.2	1.6
		0.24% HP-b-CD	0.63±0.06		4.79±0.37	2b	1.8	8.7±0.1	0.8
		1% HP-b-CD	12±2	4.0±2.9		1b		8.1±0.3	1.6
Butacaine	10.09	none	40±6	1.9±0.7		1b		8.8±0.2	1.2
	2.05	0.1M KCl	83±17	1.3±0.8		1b		8.3±0.3	1.4
		0.2M KCl	78±2	2.5±0.2		1b		8.6±0.1	0.1
		0.24% PG	51±4	2.3±0.5		1b		8.8±0.1	0.4
		1% PG	69±5	0.9±0.2		1b		8.2±0.1	0.5
		5% PG	66±9	1.5±0.5		1b		8.5±0.2	0.9
		0.24% NMP	47±3	2.1±0.5		1b		8.8±0.1	0.6
		1% NMP	71±5	1.9±0.5		1b		8.5±0.1	0.5
		0.24% PEG400	151	3.6		1b		8.5	– b
		1% PEG400	107±2	2.8±0.4		1b		8.5±0.1	0.1
		5% PEG400	107	2.8		1b		8.5	– b
		3 mM NaTC	50±10	3.1±1.6		1b		8.9±0.2	1.1
		15 mM NaTC	96±4	2.3±0.4		1b		8.5±0.1	0.2
		0.24% HP-b-CD	79±4	2.0±0.3		1b		8.5±0.1	0.3
1% HP-b-CD	141±7	1.5±0.4		1b		8.1±0.1	0.3		
clotrimazole	6.02	none	0.39±0.18		5.93±0.39	2b	1.4	7.4±1.1	2.8
		0.1M KCl	0.39		6.20±0.06	2b	1.6	7.4	0.9
		0.2M KCl	4.8±1.3	3.3±1.2		1b		5.9±0.2	1.2
		0.24% PG	1.1±0.2		4.50±0.22	2b	1.6	6.5±0.4	0.9
		1% PG	2.0±0.5		2.56±0.73	2b	2.3	6.1±0.1	1.9
		5% PG	2.6±1.0		4.65±0.53	2b	1.4	6.3±0.5	1.9
		0.24% NMP	1.3±0.2		4.59±0.25	2b	2.0	6.4±0.3	1.3
		1% NMP	1.7±0.2		4.77±0.16	2b	1.8	6.5±0.2	0.8
		0.24% PEG400	0.39		7.54±0.03	2b	1.3	7.9	0.6
		1% PEG400	0.39		7.15	2b	1.9	7.4	-b
		5% PEG400	1.9±0.6		6.86±0.12	2b	0.8	6.4±0.1	0.1
		3 mM NaTC	1.0±0.1		5.23±0.18	2b	1.5	6.4±0.2	0.9
		15 mM NaTC	20±2	6.8±1.4		1b		5.5±0.1	0.6
		0.24% HP-b-CD	17±0.4	6.6±0.4		1b		5.6±0.1	0.2
		1% HP-b-CD	85±4	11.3±2.0		1b		5.1	0.4
dipyridamole	6.22	none	6.2±1.1	2.3±0.7		1b		5.8±0.1	2.1
		0.1M KCl	5.2±0.8	3.3±0.8		1b		6.0±0.1	0.8
		0.2M KCl	5.8±0.9	3.1±0.7		1b		5.9±0.1	0.8
		0.24% PG	5.8±0.5	2.1±0.3		1b		5.8±0.1	0.5
		1% PG	6.5±0.3	2.7±0.2		1b		5.8±0.1	0.3
		5% PG	9.8±1.3	3.9±0.8		1b		5.8±0.1	0.8
		0.24% NMP	5.9±1.1	2.2±0.6		1b		5.8±0.1	1.0
		1% NMP	8.1±1.5	2.4±0.7		1b		5.7±0.1	1.1
		0.24% PEG400	4.6±1.2		6.95±0.13	2b	0.6	6.8±0.1	0.4
		1% PEG400	11±3	5.0±1.9		1b		5.9±0.2	1.3
		5% PEG400	14±1	13.7±2.4		1b		6.2±0.1	0.4
		3 mM NaTC	24±2	5.3±0.9		1b		5.6±0.1	0.5
		15 mM NaTC	110±5	9.9±1.7		1b		5.2±0.1	0.4
		0.24% HP-b-CD	7.1±0.8	2.8±0.7		1b		5.8±0.1	0.8
		1% HP-b-CD	15±1	3.2±0.7		1b		5.6±0.1	0.6
griseofulvin		none	14±0.4						
		0.1M KCl	21±1						
		0.2M KCl	19±2						

Table II. Continued

Compound	pK_a	Excipient	S_o^{APP}±SD	S_o±SD	log K_n±SD	Case	n±SD	K_a^{APP}±SD	GOF
		0.24% PG	18±2						
		1% PG	24±1						
		5% PG	25±2						
		0.24% NMP	19±1						
		1% NMP	25±1						
		0.24% PEG400	20±2						
		1% PEG400	20±1						
		5% PEG400	27±2						
		3 mM NaTC	39±2						
		15 mM NaTC	54±2						
		0.24% HP-b-CD	23±2						
		1% HP-b-CD	24±1						
progesterone		none	17±1						
		0.1M KCl	23±1						
		0.2M KCl	20±1						
		0.24% PG	18±3						
		1% PG	19±2						
		5% PG	24±14						
		0.24% NMP	14±2						
		1% NMP	20±1						
		0.24% PEG400	18±1						
		1% PEG400	15±2						
		5% PEG400	30±6						
		3 mM NaTC	22±1						
		15 mM NaTC	48±3						
		0.24% HP-b-CD	162±9						
		1% HP-b-CD	187±6						
glibenclamide	5.90	none	0.35±0.10		7.23±0.16	2a	1.1±0.1	4.3±0.1	1.4
		0.1M KCl	0.35		6.97±0.15	2a	1.1±0.2	4.3	2.7
		0.2M KCl	0.35		6.99±0.06	2a	1.2±0.1	4.3	1.1
		0.24% PG	0.35		7.36±0.12	2a	1.1±0.2	4.3	2.4
		1% PG	0.35		7.34±0.08	2a	1.1±0.1	4.3	1.7
		5% PG	0.71		7.37±0.02	2a	1.0±0.04	4.2±0.2	0.5
		0.24% NMP	0.45±0.11		6.95±0.15	2a	1.0	4.6±0.1	1.2
		1% NMP	0.65±0.10		6.92±0.08	2a	0.8±0.1	4.7±0.1	0.5
		0.24% PEG400	0.36		5.96±0.09	2a	0.9±0.2	5.4±0.1	0.6
		1% PEG400	0.26		6.88±0.09	2a	0.9±0.1	4.7±0.2	1.0
		5% PEG400	2.69		5.95±0.36	2a	0.8±0.5	5.6±0.2	1.0
		3 mM NaTC	0.32		7.42±0.03	2a	1.2±0.04	4.3±0.1	0.4
		15 mM NaTC	2.5±1.6		6.69±0.52	2a	0.5±0.2	5.5±0.1	0.5
		0.24% HP-b-CD	4.4±1.7		6.67±0.39	2a	0.9±0.2	5.1±0.1	0.6
		1% HP-b-CD	24±5		6.79±0.32	2a	0.7±0.1	5.4±0.1	0.2
mefenamic acid	4.54	none	0.021±0.005		6.02±0.80	2a	2.6±2.1	4.3±0.3	3.6
		0.1M KCl	0.023±0.005		6.61±0.60	2a	3.5	4.4±0.4	2.0
		0.2M KCl	0.021		5.72±0.38	2a	2.1±1.1	4.3	3.7
		0.24% PG	0.021		6.88±0.54	2a	3.3±1.2	4.1±0.3	1.4
		1% PG	0.021		6.46±0.72	2a	2.0±1.2	4.0±0.3	4.2
		5% PG	0.056		5.87±0.09	2a	0.9±0.1	4.0	1.0
		0.24% NMP	0.019±0.009		6.22±0.58	2a	2.0	4.1±0.6	3.4
		1% NMP	0.062±0.010		5.01±0.55	2a	2.5±1.8	4.4±0.2	1.3
		0.24% PEG400	0.004±0.002		5.15±1.08	2a	2.5	4.5±0.2	4.4
		1% PEG400	0.021			2a		4.5	1.1
		5% PEG400	0.028		4.98±0.58	2a	0.6	4.5±1.1	1.7
		3 mM NaTC	1.9±0.4	0.11±0.03		1a		5.8±0.1	0.4
		15 mM NaTC	1.4±0.3	0.10±0.03		1a		5.7±0.1	1.0
		0.24% HP-b-CD	0.34±0.02	0.28±0.02		1a		4.6±0.1	0.2
		1% HP-b-CD	2.9±0.5	0.61±0.17		1a		5.2±0.1	1.1

The pK_a values are taken from (29). *SD*=standard deviation. S_o^{APP} is the apparent intrinsic solubility. S_o is the intrinsic solubility. Blank entries in the S_o field indicate that $S_o = S_o^{APP}$. The aggregation constant, log K_n is of the case indicated by the 'Case' column, with reference to the symbols in Table I. The refined order of aggregation is indicated by n. Entries without SD were determined by manual adjustment, to produce the lowest values of GOF. The pK_a^{APP} value was determined by applying the Henderson–Hasselbalch equation to the log *S*–pH data. GOF is the goodness-of-fit (Eq. 11).

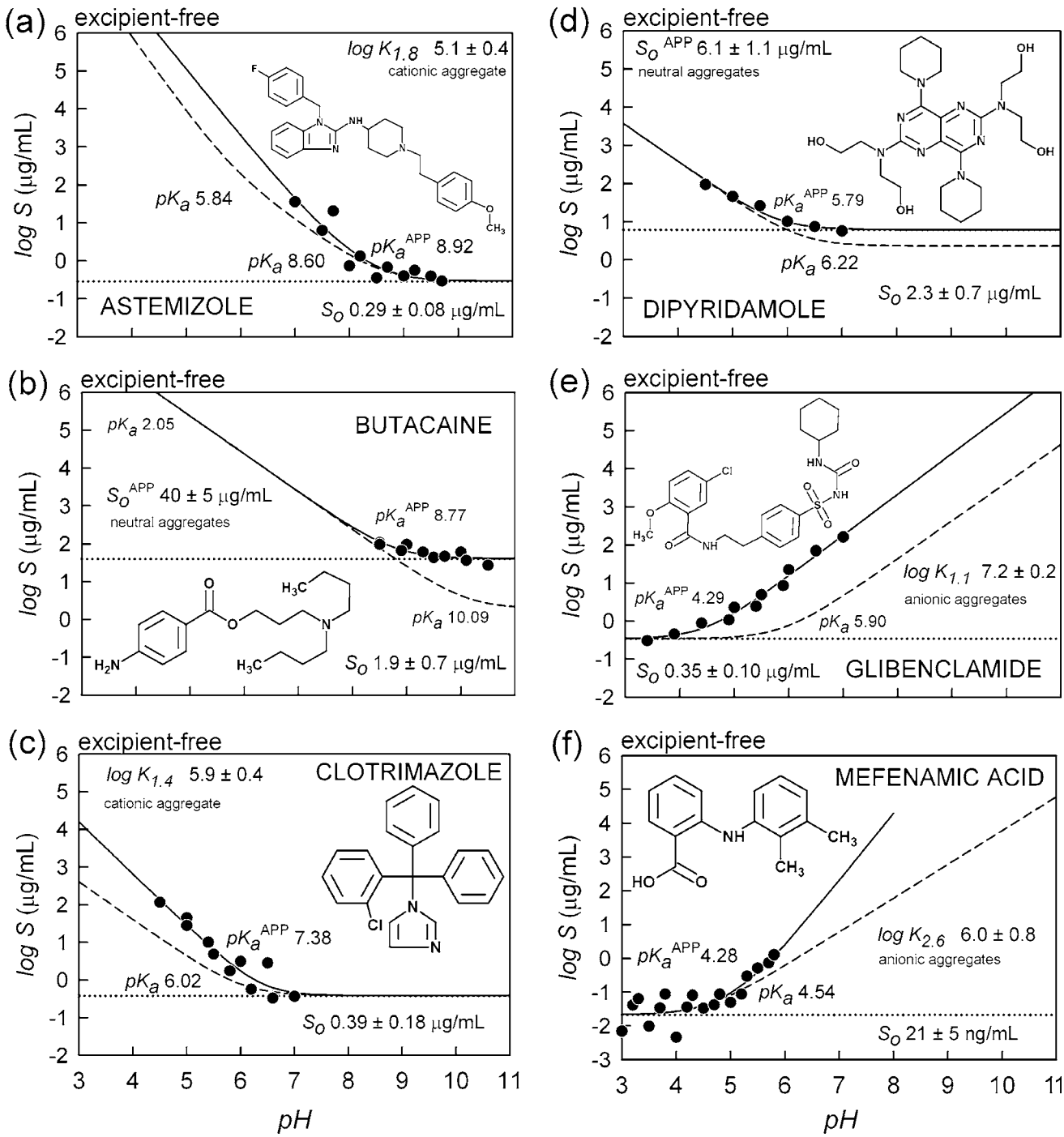

Fig. 2. Plots of log solubility *vs.* pH in excipient-free aqueous solutions for model ionizable drugs (solutions contain 1% v/v DMSO). *S* refers to the solubility in μg/ml units. The *dashed curves* were calculated with the Henderson–Hasselbalch equation, using the true pK_a values (Table II). The *solid curves* are the best-fit to the solubility data (*filled circles*), according to the aggregation model equations in Table I. The *dotted horizontal line* marks the apparent intrinsic solubility value.

Micro Solubility Measurements with Excipients

Solubility-Excipient–pH Plots

Figures 3, 4 and 5 show some of the log *S*–pH curves for the ionizable molecules studied, at one of the excipient concentrations (1% and 15 mM). The results of the other excipient concentrations considered are summarized in Table II. In addition to the curves in the excipient-free plots (Figs. 2, 3, 4 and 5), have the additional "dash-dot-dot" curves, which represent the solid curves from the excipient-free case. This transferred baseline curve allows for quick visual assessment of the impact of the excipient on a particular compound.

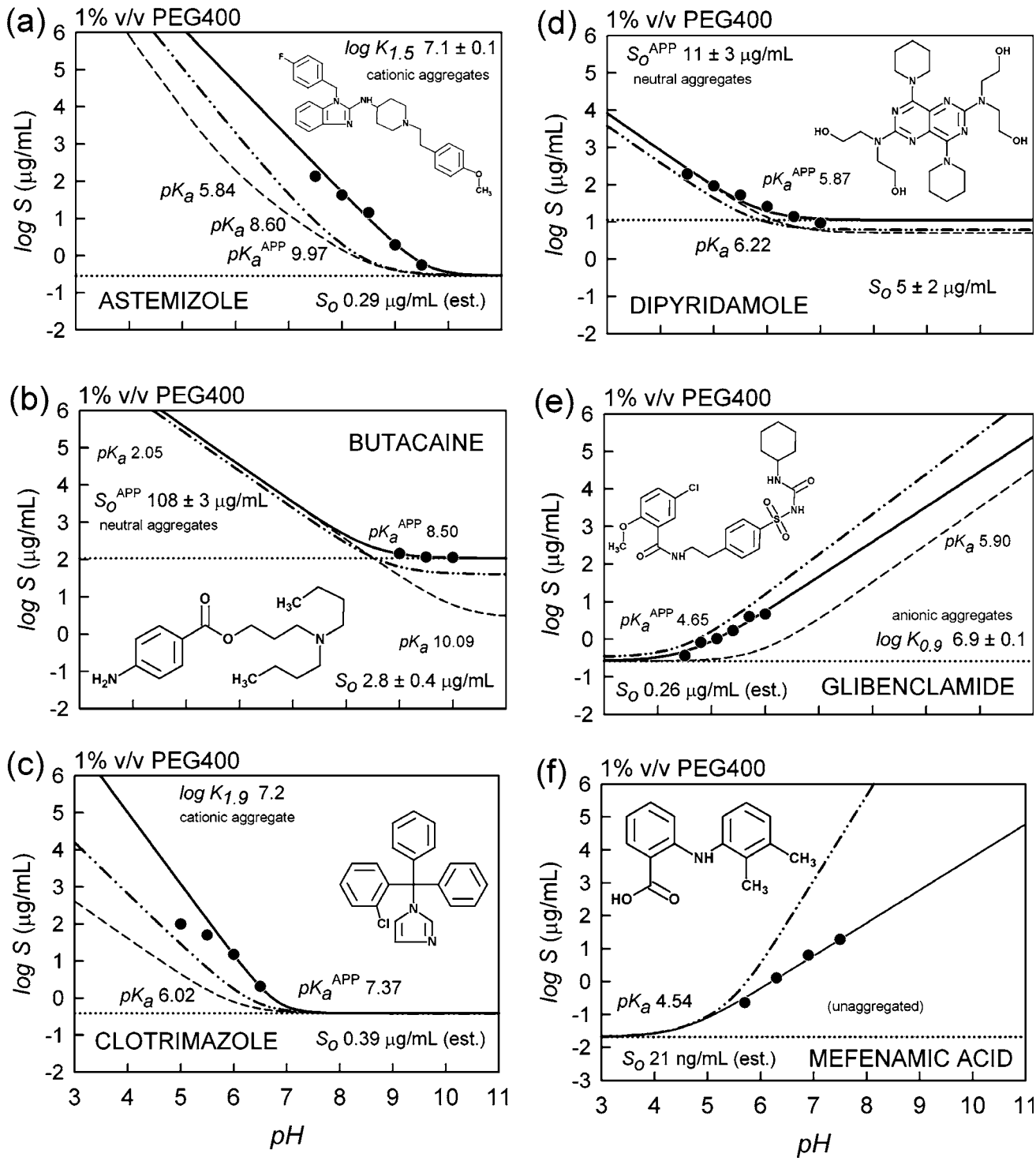

Fig. 3. Plots of log solubility *vs.* pH with 1% v/v PEG400 for model ionizable drugs (solutions also contain 1% v/v DMSO). The *dashed curves* were calculated with the Henderson–Hasselbalch equation, using the true pK_a values (Table II). The *solid curves* are the best-fit of the data (*filled circles*), according to the aggregation model equations in Table I. The *dotted horizontal line* marks the apparent intrinsic solubility value. The *dash-dot-dot curve* refers to the excipient-free best-fit curve shown in Fig. 2.

Potassium Chloride

In the presence of 0.1 and 0.2 M KCl, solubility–pH profiles are similar to those in the excipient-free cases (Fig. 2).

The apparent intrinsic solubility of only butacaine and clotrimazole are significantly elevated by 0.2 M KCl. The origin of this effect is not clear. The expected change due to "salting out" is to have a decrease in solubility, opposite of what is observed. Potassium chloride raises the ionic strength of the solution. The pK_a of the bases are not normally expected to change significantly as a result of elevation of ionic strength from 0.01 to 0.21 M (3). Ionic strength changes

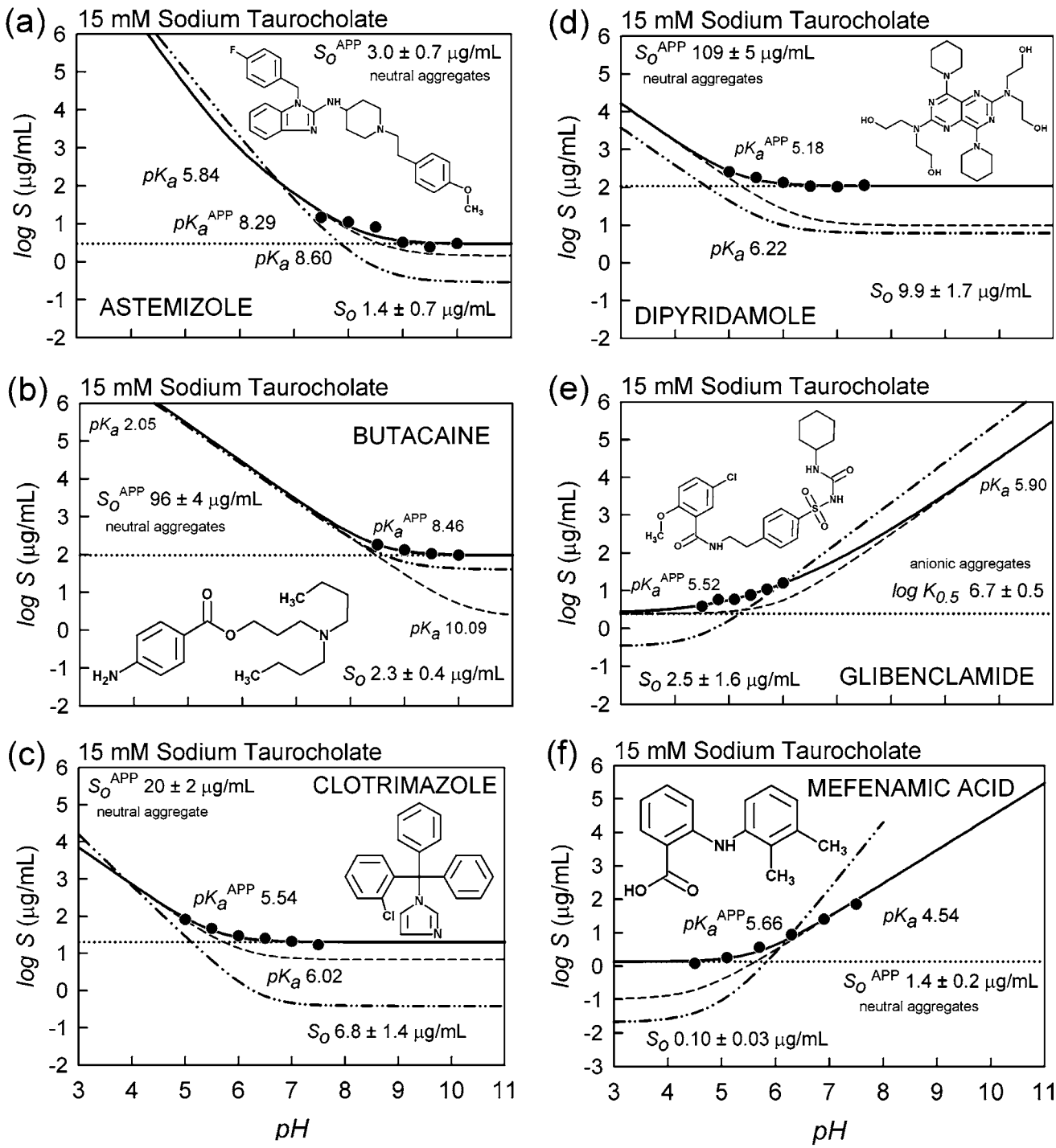

Fig. 4. Plots of log solubility *vs.* pH with 15 mM NaTC for model ionizable drugs (solutions also contain 1% v/v DMSO). The *dashed curves* were calculated with the Henderson–Hasselbalch equation, using the true pK_a values (Table II). The *solid curves* are the best-fit of the data (*filled circles*), according to the aggregation model equations in Table I. The *dotted horizontal line* marks the apparent intrinsic solubility value. The *dash-dot-dot curve* refers to the excipient-free (*solid*) curve shown in Fig. 2.

can alter the pH of the solution, but the analysis of butacaine and clotrimazole largely drew on data from the flat regions of the log *S*–pH curve, least dependent on pH uncertainty.

Astemizole seems to show a steeper pH dependence in neutral pH solutions, putatively arising from the formation of higher-order aggregates. Clotrimazole seems to show the opposite effect: the presence of high-salt concentration seems to break up the aggregates seen in excipient-free solution. Its behavior in 0.2 M KCl is well predicted by the Henderson–Hasselbalch equation. Also, its intrinsic solubility lifts from 0.39 to 3.3 μg/ml. The effect of 0.2 M KCl on dipyridamole, glibenclamide, and mefenamic acid appear minimal. The deflection of points from the curve for pH > 6.5 for mefenamic acid could be due to salt formation between K^+ and the ionized drug.

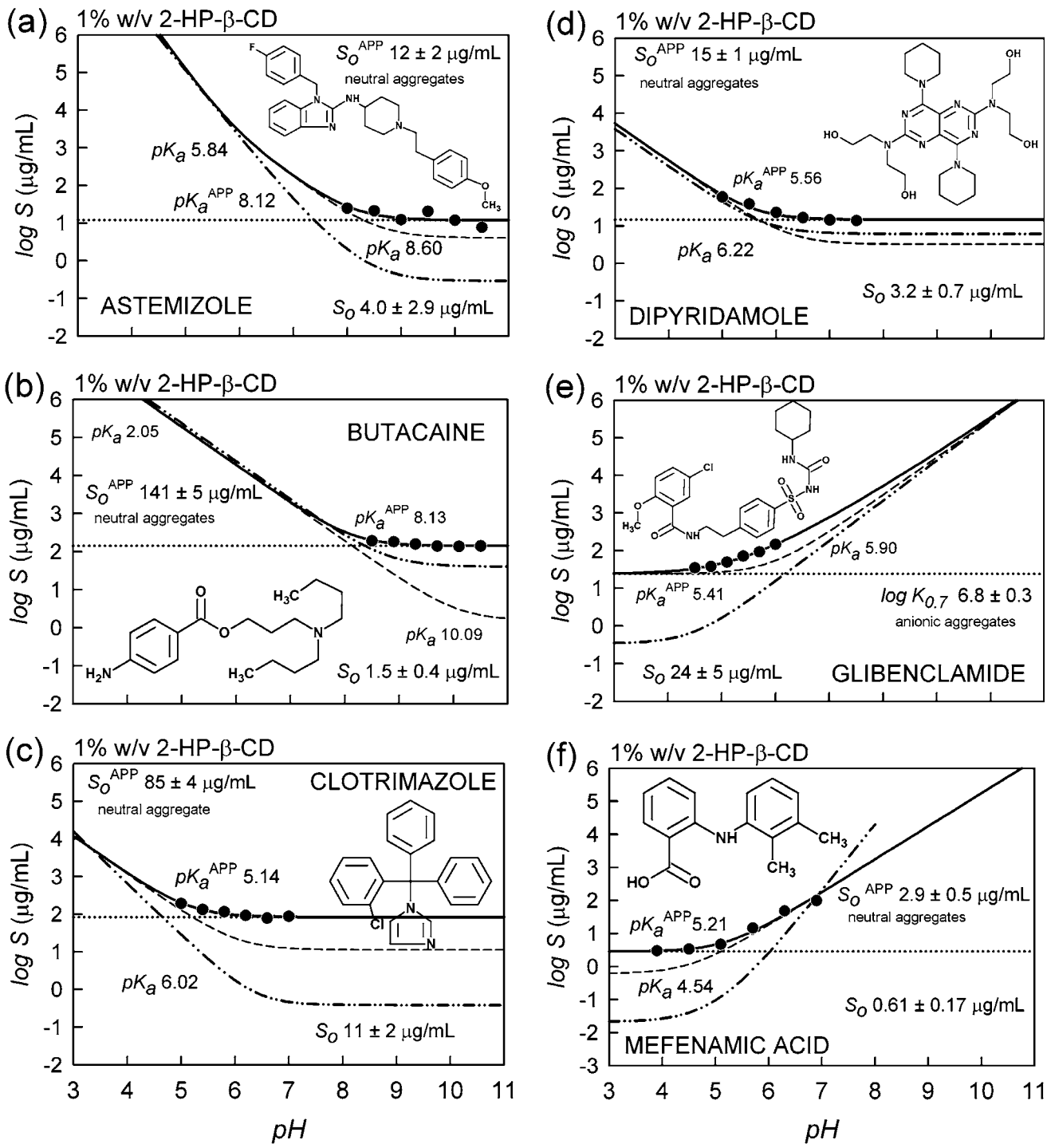

Fig. 5. Plots of log solubility *vs.* pH with 1% w/v HP-β-CD for model ionizable drugs (solutions also contain 1% v/v DMSO). The *dashed curves* were calculated with the Henderson–Hasselbalch equation, using the true pK_a values (Table II). The *solid curves* are the best-fit of the data (*filled circles*), according to the aggregation model equations in Table I. The *dotted horizontal line* marks the apparent intrinsic solubility value. The *dash-dot-dot curve* refers to the excipient-free (*solid*) curve shown in Fig. 2.

Propylene Glycol

In the presence of 1–5% PG, solubility–pH profiles are similar to those in the excipient-free cases (Fig. 2). The effects are similar to those due to 0.1–0.2 M KCl. Astemizole appears to show even higher-order aggregates (n=3.6), along with a slight decrease in intrinsic solubility. The solubility appears to increase only in low-pH solutions for astemizole. The intrinsic solubility of clotrimazole increases from 0.39 to 2.0 μg/ml.

1-Methyl-2-Pyrrolidone

In the cases of 1–5% NMP, the aggregation order diminishes in astemizole and glibenclamide, compared to KCl and PG excipients. The other effects are comparatively

smaller in degree. Clotrimazole appears to be enhanced in solubility with NMP, as with KCl and PG. Mefenamic acid responds to NMP with a slight increase in intrinsic solubility (cf., Table II).

Propylene Glycol 400

Whereas the first three excipients discussed are associated with weak effects, PEG400, with solubility–pH plots shown in Fig. 3, has a moderate impact. The binding constant of aggregation in astemizole and clotrimazole (but not the order of aggregation) greatly increase, as indicated by dramatic shifts of the solid curves to higher pH values. The aggregation in mefenamic acid appears to disappear, and the curve has classic Henderson–Hasselbalch behavior. The apparent intrinsic solubility of the more soluble drugs, dipyridamole and butacaine, nearly doubled over values shown in the previous three weaker-acting excipients.

Sodium Taurocholate

Figure 4 shows the effect of 15 mM NaTC bile salt. The patterns of effect for each of the considered drugs are dramatic, with an across-the-board elevation of solubility, particularly in the case of mefenamic acid (cf., Table II). Astemizole behaves as a classical Henderson–Hasselbalch-obeying molecule, as do all the other molecules, except glibenclamide. The latter molecule shows pH dependency slope of +0.5, which may be best described by Case 3ax behavior. Most of the aggregation-prone molecules are strongly bound to NaTC micelles, apparently as uncharged monomers, whose pH dependence can be described by the Henderson–Hasselbalch equation. The analysis of the apparent binding strength (3,23,24) can be described by Case 1a or 1b equations (Table I).

2-Hydroxypropyl-β-Cyclodextrin

As with the bile salt, 1% HP-β-CD, has the tendency to break up aggregates, as shown in Fig. 5. Although we have chosen to represent the solubility equilibria with an aggregation model, the association is that of complexation. The aggregation model is still convenient in categorizing the solubility effects, in order to compare this to the action of the other excipients with a similar model. (General complexation models based on the analysis of phase-solubility diagrams will be the subject of a future study.) Both the bile salt and the cyclodextrin have a significant effect on elevating solubility of the drugs studied. Both excipients appear to diminish the formation of aggregates. Glibenclamide still has the unique half-integral slope value in the solubility–pH plot (Fig. 5e).

Astemizole

Table II is a convenient reference in comparing the effects of all the excipients on a particular drug. In the case of astemizole, solubility is greatly enhanced by 1% HP-β-CD (excipient-free value of 0.29 μg/ml raised to 12 μg/ml) and also by 15 mM NaTC. The strength of aggregation (log K_n/n) is elevated most significantly by 0.24% and 5% PEG400, over values in excipient-free solutions. Slightly lesser elevations are noted with 1% PEG400 and 1% NMP.

Butacaine

Butacaine does not appear to form charged aggregates. The solubility of the most soluble molecule of those considered here is most easily elevated by not only both of the HP-β-CD concentrations (Table II), but also by 0.1 M KCl, all PEG400 concentrations (excipient-free value of 40 μg/ml raised to 152 μg/ml), and 15 mM NaTC.

Clotrimazole

As with astemizole, the aggregates with clotrimazole are widely affected by various excipients. The strength of aggregation (log K_n/n) is significantly elevated by 0.24% and 5% PEG400. The biggest gains in solubility come from the use of 15 mM NaTC and 1% HP-β-CD (excipient-free value of 0.39 μg/ml raised to 85 μg/ml).

Dipyridamole

The PEG400 aggregation strengthening effect is seen with dipyridamole at the low excipient concentration. Solubility is elevated to 110 μg/ml from the excipient-free value of 6.2 μg/ml by 15 mM NaTC. Other excipients have significant effects on solubility (cf., Table II).

Griseofulvin

Aggregation phenomena cannot be indicated by the "pK_a-shift" method, since both griseofulvin and progesterone are non-ionizable. The elevation of solubility takes place with the "strong" excipients: excipient-free value of 14 μg/ml is raised to 54 μg/ml by 15 mM NaTC. The impact of the excipients on the solubility of griseofulvin is relatively less dramatic than that on other lesser soluble drugs studied.

Progesterone

In contrast to griseofulvin, progesterone is strongly affected by cyclodextrin. As with griseofulvin, the elevation of solubility takes place with the "strong" excipients: but the excipient-free value of 17 μg/ml is raised to 187 μg/ml by 1% HP-β-CD with progesterone.

Glibenclamide

The strength of aggregation with glibenclamide is only increased by the excipients, especially 15 mM NaTC. This may be a "salting-out" phenomenon, appearing consistently with PEG400. This is a new and unexpected observation, and will require further investigation.

Mefenamic Acid

With the least soluble drug of the set studied, the best enhancement to solubility is effected by NaTC and HP-β-CD, but the highest intrinsic solubility achieved is still relatively

low, less than 3 μg/ml. NMP and PEG seem to increase the aggregation strength (log K_n/n).

Summary of Solubility-Excipient Trends

It is not surprising that excipients raise the solubility of sparingly soluble molecules, as illustrated in this study. Perhaps what is new is that the extent and nature of such effects can be very quickly and reliably assessed by the robotic instrument used. By comparisons of our results to those derived from DMSO-free shake-flask methods (next section), our values appear acceptably accurate, in spite of the presence of 1% DMSO in all of the solutions in this study.

Considering the effects of specific excipients, perhaps the new observation is that PEG400 (and to a lesser extent, NMP) seems to increase the strength of aggregation (log K_n/n) of a number of the drugs. We are not familiar with any previous such observations in the literature. The nature of the interactions are not entirely understood, but perhaps it is useful to consider the following possible effect. The moderate strength PEG400 may not provide a sufficiently competitive hydrophobic environment into which to attract the drugs, compared to that of cyclodextrin and sodium taurocholate. However, the 1% DMSO present in all solutions and some water of solvation may be attracted to the PEG400 molecules, making the excipient- and DMSO-poor residual portion of the buffer solution more concentrated in the drug aggregates, leading to their stronger self-associations. We are using the analogy of the "salting out" effect here. This speculative view will require further testing.

Comparisons to Literature Determinations of the Solubility–pH Behavior of the Studied Drugs

Glomme *et al.* (9) published solubility–pH data for dipyridamole, glibenclamide, and mefenamic acid, at 37°C. Bergström *et al.* (11) published such data for dipyridamole, at 23°C. Both studies were performed by miniaturized shake-flask procedures, with DMSO-free buffer solutions. Figure 6 shows the data from the literature, fitted with equations from Table I, and comparing to the results obtained by us in excipient-free solutions (dash-dot-dot curves in Fig. 6). Salt formation appears in glibenclamide and mefenamic acid at elevated pH, and at low pH for dipyridamole (Fig. 6d). Our

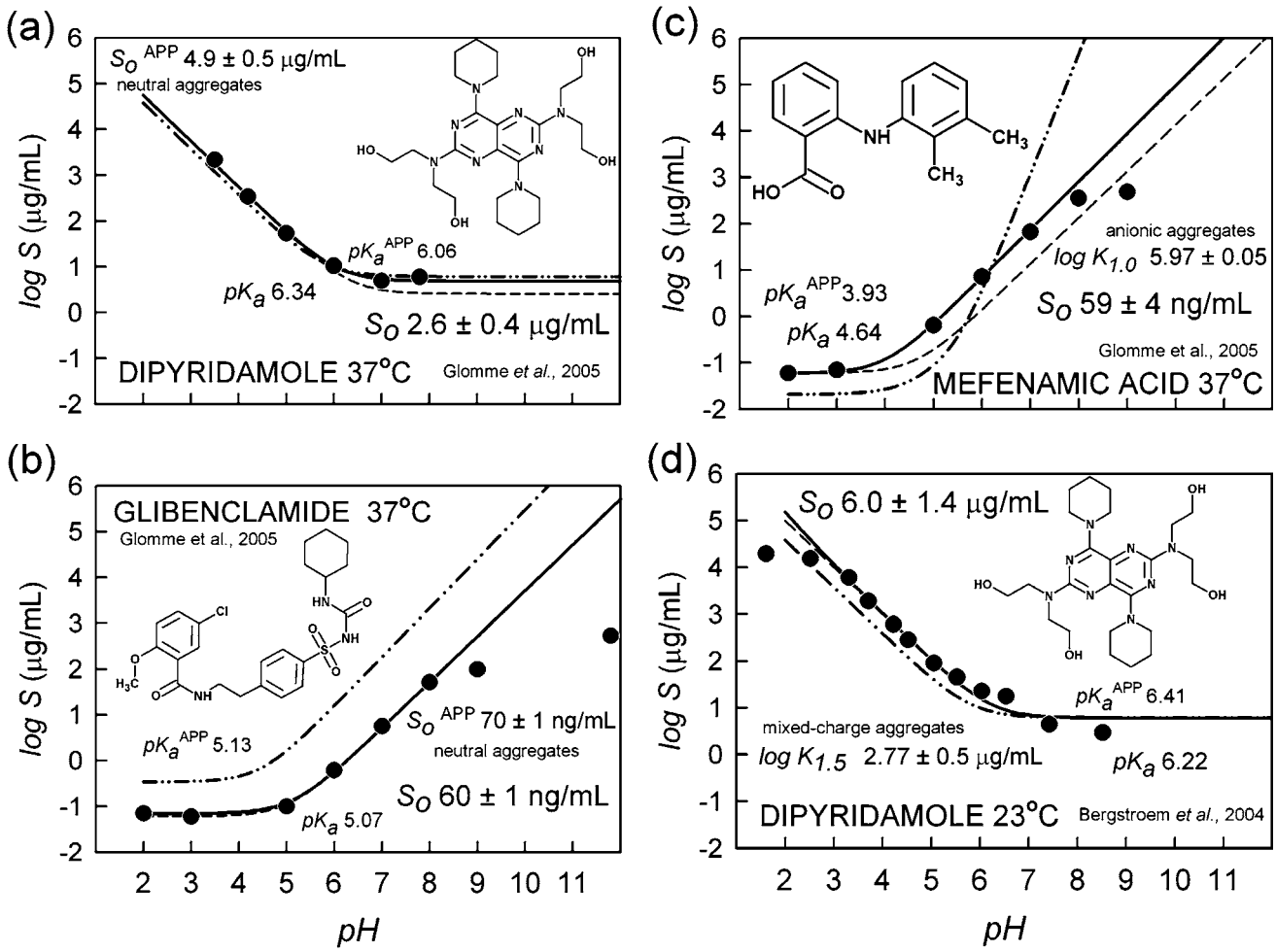

Fig. 6. Literature values (9,11) of log *S vs.* pH of compounds in this study. *Solid curves* represent the aggregation equation (Table I) analysis of the reported measurements. The *dash-dot-dot curve* refers to the excipient-free (*solid*) curve shown in Fig. 2. The *dashed curves* were calculated with the Henderson–Hasselbalch equation, using the true pK_a values from Table II for the 23°C data (11). The 37°C pK_a values used in the calculation for the literature measurements, listed in the figure, were deconvoluted from the reported *p*SOL log *S vs.* pH values (data not shown) in (9).

dipyridamole results agree almost perfectly with those of Glomme *et al.*, and very closely with those of Bergström *et al.* The apparent intrinsic solubility of glibenclamide in the literature, 70±1 ng/ml, is lower than what we have determined, 350±100 ng/ml. This may be due to the presence of 1% DMSO in our solutions. However, our intrinsic result with mefenamic acid is lower than that of the literature (Fig. 6c). Also, we see aggregates at 25°C, but these are less apparent in the 37°C data of Glomme *et al.*, consistent with previous observations that aggregation is temperature sensitive (14,15,21). The dipyridamole example at 23°C (Fig. 6d) indicates mixed-charge aggregation. Considering how much variance is usually seen in published shake-flask solubility values, the relatively good agreement between our results (with 1% DMSO in all solutions) and those published in the literature, performed by the more rigorous shake-flask method, in the absence of any DMSO, makes us confident that the robotic method described here is capable of producing accurate solubility measurements, at high speed, with minimal consumption of sample.

Rank-Ordered Intrinsic Solubility-Excipient (ISE) Classification Gradient Map

As we did in our previous PAMPA-excipient study (29), we propose in this study a classification gradient mapping scheme shown in Fig. 7 (ISE-Mapping), which improves the visualization of the excipient effects, allowing for precise systematic evaluation. The map can be automatically generated by the software associated with the solubility instrument used in the study. Plotted in Fig. 7 are apparent intrinsic log solubility ratios, with excipient solubility divided by excipient-free base value. Such a "gradient" map normalizes solubility to shift patterns with reference to the excipient-free baseline. Since 1% DMSO is present in all solutions, a gradient map is expected to eliminate some of the impact of DMSO. In Fig. 7, green values represent the base (unaffected) values. Warm colors (yellow to deep orange) represent enhanced intrinsic solubility, and cool colors (deep blue) refer to depressed values. Along the vertical axes are the excipient compositions, rank ordered by decreasing average intrinsic solubility enhancement. Along the horizontal axes are the drugs, arranged in the order decreasing benefit due to excipients. The top left corner represents the "best" combination of excipients and compounds. The lower right corner represents the "worst" combination. With this intrinsic solubility-excipient (ISE) classification gradient map procedure, or ISE-Mapping for short, it would be very efficient to recognize and thus prioritize the most promising molecule-excipient combinations, and such ISE-Mapping can be applied to a very large numbers of molecules, as are encountered in discovery-optimization programs in pharmaceutical companies.

The three most helpful excipients in this study appear to be 1% HP-β-CD, 15 mM NaTC, and 0.24% HP-β-CD. The least-effective excipients are 0.24% PEG400, 0.1M KCl, and 0.24% PG. From Fig. 7, it is visually apparent that clotrimazole, with its overall "warm" colored vertical track in the map, is ranked relatively high. Not only is intrinsic solubility

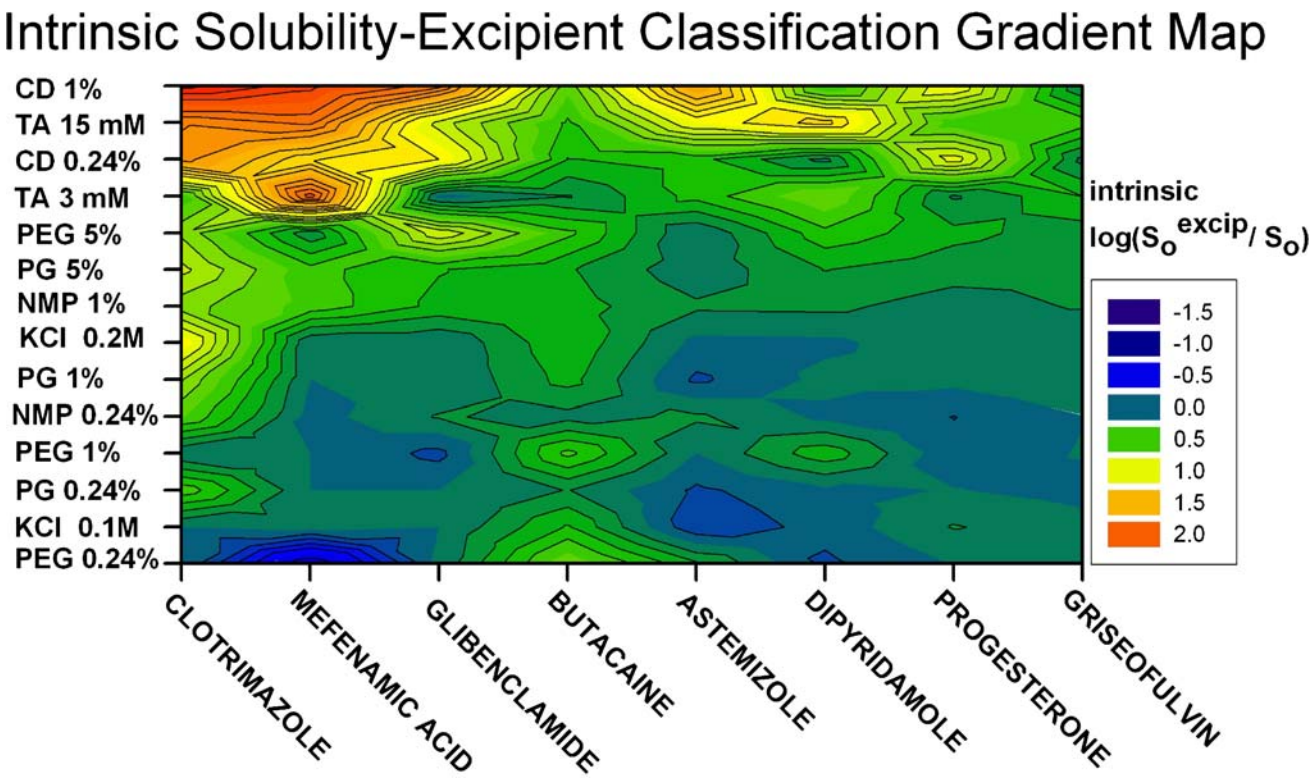

Fig. 7. Rank-ordered classification gradient map for the compounds and excipient combinations studied. The values in the contour map are logarithm of the ratio of the apparent intrinsic solubility to the apparent excipient-free value, i.e., the baseline value. *Warm colors* refer to excipient-enhanced solubility, and *cool colors* refer to excipient-depressed solubility, with *dark green* being the base value. The excipient rows are sorted according to descending order of enhancement of solubility, and the molecule columns are sorted in descending order of enhanced solubility.

enhanced by the strong excipients, such as 1% HP-β-CD, it is also elevated by moderate and relatively weak excipients, such as 0.2 M KCl. As ISE-Mapping indicates, the solubility enhancement of progesterone and griseofulvin is weak and comparable in magnitude, and these two molecules are classed to the right side of the map. Only at the top of the map does progesterone shows some warm color effects, differentiating itself slightly from griseofulvin.

CONCLUSION

We conclude that we have met the objectives of our study: to develop a practical, low-cost and reasonably accurate high-throughput assay method which could be used in early screening for intrinsic solubility in the presence of excipients. This is thought to be beyond the capability of turbidity-based solubility methods (9,10). The classification gradient mapping procedure (ISE-Mapping) introduced in this study may prove to be very useful ranking tool in the future, as more compounds are characterized.

REFERENCES

1. H. van de Waterbeemd, D. A. Smith, K. Beaumont, and D. K. Walker. Property-based design: optimization of drug absorption and pharmacokinetics. *J. Med. Chem.* **44**:1313–1333 (2001).
2. H. Waterbeemdvan de, D. A. Smith, and B. C. Jones. Lipophilicity in PK design: methyl, ethyl, futile. *J. Comp.-Aided Molec. Des.* **15**:273–286 (2001).
3. Avdeef, A. *Absorption and Drug Development*. Wiley, New York, 2003, pp. 116–246.
4. C. A. Lipinski. Drug-like properties and the causes of poor solubility and poor permeability. *J. Phamacol. Tox. Methods* **44**:235–249 (2000).
5. C. Lipinski. Poor aqueous solubility—an industry wide problem in drug discovery. *Amer. Pharm. Rev.* **5**:82–85 (2002).
6. Pharma Algorithms, Toronto, Canada. Algorithm Builder V1.8 and ADME Boxes V2.5 computer programs (http://www.ap-algorithms.com; date accessed 7 September 2006).
7. Advanced Chemistry Development Inc., Toronto, Canada. ACD/Solubility DB computer program (http://www.acdlabs.com; date accessed 16 January 2006).
8. W. M. Maylan and P. H. Howard. Estimating log P with atom/fragments and water solubility with log P. *Perspect. Drug Discov. Des.* **19**:67–84 (2000).
9. A. Glomme, J. März, and J. B. Dressman. Comparison of a miniaturized shake-flask solubility method with automated potentiometric acid/base titrations and calculated solubilities. *J. Pharm. Sci.* **94**:1–16 (2005).
10. B. Faller and F. Wohnsland. Physicochemical parameters as tools in drug discovery and lead optimization. In:B, Testa, H. van de Waterbeemd, G. Folkers, and R. Guy (eds.), *Pharmacokinetic Optimization in Drug Research*, Verlag Helvetica Chimica Acta, Zürich and Wiley—VCH, Weinheim, 2001, pp. 257–274.
11. C. A. S. Bergström, K. Luthman, and P. Artursson. Accuracy of calculated pH-dependent aqueous drug solubility. *Eur. J. Pharm. Sci.* **22**:387–398 (2004).
12. V. Bakatselou, R. C. Oppenheim, and J. B. Dressman. Solubilization and wetting effects of bile salts in the dissolution of steroids. *Pharm. Res.* **8**:1461–1469 (1991).
13. T. Higuchi, F.-M. Shih, T. Kimura, and J. H. Rytting. Solubility determination of barely aqueous-soluble organic solids. *J. Pharm. Sci.* **68**:1267–1272 (1979).
14. W. H. Streng, D. H.-S. Yu, and C. Zhu. Determination of solution aggregation using solubility, conductivity, calorimetry, and pH measurement. *Int. J. Pharm.* **135**:43–52 (1996).
15. C. Zhu and W. H. Streng. Investigation of drug self-association in aqueous solution using calorimetry, conductivity, and osmometry. *Int. J. Pharm.* **130**:159–168 (1996).
16. S. W. Smith and B. D. Anderson. Salt and mesophase formation in aqueous suspensions of lauric acid. *Pharm. Res.* **10**:1533–1543 (1993).
17. A. Fini, G. Fazio, and G. Feroci. Solubility and solubilization properties of non-steroidal antiinflammatory drugs. *Int. J. Pharm.* **126**:95–102 (1995).
18. Y. Bouligand, F. Boury, J.-M. Devoisselle, R. Fortune, J.-C. Gautier, D. Girard, H. Maillol, and J.-E. Proust. Ligand crystals and colloids in water–amiodarone systems. *Langmuir* **14**:542–546 (1998).
19. T. J. Roseman and S. H. Yalkowsky. Physicochemical properties of prostaglandin $F_{2\alpha}$ (tromethamine salt): solubility behavior, surface properties, and ionization constants. *J. Pharm. Sci.* **62**:1680–1685 (1973).
20. J. Jinno, D.-M. Oh, J. R. Crison, and G. L. Amidon. Dissolution of ionizable water-insoluble drugs: the combined effect of pH and surfactant. *J. Pharm. Sci.* **89**:268–274 (2000).
21. A. Avdeef, D. Voloboy, and A. Foreman. Dissolution–Solubility: pH, Buffer, Salt, Dual-Solid, and Aggregation Effects. In B. Testa, and H. van de Waterbeemd (eds.), *Comprehensive Medicinal Chemistry II*, vol. 5 ADME-TOX Approaches. Elsevier, Oxford, UK, 2006, in press.
22. A. Avdeef. High-throughput measurements of solubility profiles. In B. Testa, H. van de Waterbeemd, G. Folkers, and R. Guy (eds.), *Pharmacokinetic Optimization in Drug Research*, Verlag Helvetica Chimica Acta: Zürich and Wiley, Weinheim, 2001, pp. 305–326.
23. A. Avdeef. Physicochemical Profiling (Permeability, Solubility, Charge State). *Curr. Topics Med. Chem.* **1**:277–351 (2001).
24. A. Avdeef and B. Testa. Physicochemical profiling in drug research: a brief state-of-the-art of experimental techniques. *Cell. Molec. Life Sci.* **59**:1681–1689 (2003).
25. K. Okimoto, R. A. Rajewski, K. Uekama, J. A. Jona, and V. J. Stella. The interaction of charged and uncharged drugs with neutral (HP-β-CD) and anionically charged (SBE7-β-CD) β-cyclodextrins. *Pharm. Res.* **13**:256–264 (1996).
26. X. Wen, Z. Liu, T. Zhu, M. Zhu, K. Jiang, and Q. Huang. Evidence for the 2:1 molecular recognition and inclusion behavior between β- and γ-cyclodextrins and cinchonine. *Bioorg. Chem.* **32**:223–233 (2004).
27. H. Liu, C. Sabus, G. T. Carter, C. Du, A. Avdeef, and M. Tischler. *In vitro* permeability of poorly aqueous soluble compounds using different solubilizers in the PAMPA assay with liquid chromatography/mass spectrometry detection. *Pharm. Res.* **20**:1820–1826 (2003).
28. H. Chen, Z. Zhang, C. McNulty, O. Cameron, H. J. Yoon, J. W. Lee, S. C. Kim, M. H. Seo, H. S. Oh, A. V. Lemmo, S. J. Ellis, and K. Heimlich. A high-throughput combinatorial approach for the discovery of a Cremophor EL-free paclitaxel formulation. *Pharm. Res.* **20**:1302–1308 (2003).
29. S. Bendels, O. Tsinman, B. Wagner, D. Lipp, I. Parrilla, M. Kansy, and A. Avdeef. PAMPA-Excipient Classification Gradient Maps. *Pharm. Res.* **23**:2525–2535 (2006).
30. Beckman Coulter, Inc., Fullerton, CA, USA. Biomek® FX Automated Assay Optimization (http://www.beckman.com; date accessed 16 January 2006).
31. P. Taylor. Optimising assays for automated platforms. *Modern Drug Discov.* December issue, 37–39 (2002).
32. H. Tye. Application of statistical 'design of experiments' methods in drug discovery. *Drug Discov. Today* **9**:485–491 (2004).
33. A. S. Uch, U. Hesse, and J. B. Dressman. Use of 1-methylpyrrolidone as a solubilizing agent for determining the uptake of poorly soluble drugs. *Pharm. Res.* **16**:968–971 (1999).
34. E. Rytting, K. A. Lentz, X.-Q. Chen, F. Qian, and S. Venkatesh. Aqueous and cosolvent solubility data for drug-like organic compounds. *The AAPS J.* **7**:E78–E105 (2005).(http://www.aapsj.org; date accessed 7 December 2005).
35. J. B. Dressman. Dissolution testing of immediate-release products and its application to forecasting *in vivo* performance. In J. B. Dressman, and H. Lennernäs (eds.), *Oral Drug Absorption*, Dekker, New York, 2000, pp. 155–181.
36. A. Avdeef and J. J. Bucher. Accurate measurements of the concentration of hydrogen ions with a glass electrode: calibrations using the Prideaux and other universal buffer solutions and a computer-controlled automatic titrator. *Anal. Chem.* **50**:2137–2142 (1978).